Pore Pressure and Fracture Gradient Modelling in Northwest Khilala Field, Onshore Nile Delta, Egypt.

A. Aly, W. Saleh
Exploration Division
Suez Oil Company, SUCO-Egypt, Cairo Egypt
Amany.Aly@suco-eg.com

A. AbdelHalim, M. Hammed
Geology Department
Faculty of Science Cairo University, Giza Egypt
salehhammed@cu.edu.eg

Abstract

Modeling of Pore Pressure and Fracture Gradients (PPFG) of the hydrocarbon-bearing clastic successions are crucial in the drilling risk assessment and geomechanical reservoir modeling during the entire field lifetime. There are various estimation techniques of the PPFG based on borehole logs of good clues during drilling (predrill and while drilling) with variable uncertainties.

The Northwest Khilala (NWK) gas field lies in the central onshore part of the extensively exploited hydrocarbon province of the Miocene Nile Delta. The present study aims to construct a 1D PPFG model by using the logging data of four penetrations in the field. The results of the Eaton and K0 methods are assessed and calibrated with actual MDT and MW data to evaluate their accuracy and limitation. The estimated pore pressure model of the NWK gas field is classified into three types of pressure regimes that are 1) A normal-pressure regime, 2) an overpressured regime with a hydrostatic gradient and 3) an overpressured regime with an overpressure gradient. The top of overpressure is indicated by departure from normal trend (NCT) at depth ~1900 m TVDss where a slightly over-pressured gradient starts within Late Pliocene Kafr El-Sheikh Formation and increases gradually to reach the maximum (~5260 psi) at the base. The pore pressure gradient increases gradually to display a regression/transgression cycle in the Late Miocene Abu-Madi Formation followed by a significant increase and pressure ramp in the Qawasim Formation of the NWK1X &NWK1-2 wells. It is concluded that the wireline Resistivity log was inefficient to identify the Qaswasim pressure ramp. The constructed model can extend to give clues and be applied in the nearby fields of the Nile Delta.

Keywords— Pore pressure, Nile Delta, Northwest Khilala, Fracture gradient

1. INTRODUCTION

The Pore Pressure and Fracture Gradients (PPFG) affect the technical merits as well as the financial aspect of the well plan (Chennakrishnan, 2008). The PPFG is essential to ensure safe drilling operations and is a fundamental input into the well design, particularly the selection of casing points (Law and Spencer, 1998). The Pressure vs. Depth plot is a vital document displaying changes in pressure and all other related data such as the mud weight, fracture pressure, mud losses and gains (Mouchet and Mitchell, 1989;). The methods of pore-pressure prediction involve indirect quantifying from rock property variations as reflected by changes in sonic, velocity, and resistivity logs (Mouchet and Mitchell, 1989; Hottman & Johnson, 1965; Eaton, 1975). Wire log data are one of the most reliable and valuable sources of data, which contains useful information helping formation pore-pressure prediction and assessment as mentioned by Fertl (1976). There are several causes for overpressured sediments among them the compaction disequilibrium, where the overburden pressure makes compaction on underlying sediments and fluids are unable to expel to reach hydrostatic pressure due to the high rate of sedimentation (Fertl, 1976; Law and Spencer, 1998; Osborne & Swarbrick, 1997.). As a result of the sedimentation history following delta evolution such as Niger, Vietnamese and Mekong Deltas are commonly associated with accelerating in natural compaction and consequently pore pressure disequilibrium. The Miocene to Holocene clastic sedimentary sequences of the Nile Delta of Egypt is mainly derived from marine and deltaic channels and are predominantly clastics of sands and clays where the possibilities of overpressure shale intervals and lateral and vertical compartmentalization are high. The main causes of abnormal pressure in the Nile Delta are attributed mainly to the disequilibrium compaction and the subordinate fluid expansions in the Oligo-Miocene compartment due to aqua thermal, hydrocarbon generation, and thermal cracking (Nashaat et al., 1998). Herein, we present a pore pressure and fracture gradients modeling by applying the various theoretical approaches on available logging data of the Northwest Khilala (NWK) gas field. This allows us to have an accurate predrill prediction with less uncertainty and compartmentalization styles within the highly exploited gas-bearing sediments of the Miocene Nile Delta province in general and the studied field.

2. GEOLOGIC SETTING

The Nile Delta is the type locality of the World deltas and presents one of the main petroleum provinces in Egypt (EGPC, 1994, Said, 1990). Structurally, the Nile delta has been subdivided into four structural sedimentary provinces (Sestini,1984; Ross and Uchupi,1977) namely as (i) the south Delta province, a continuation of western desert stratigraphic sequence and structures, (ii) the north delta basin, is bounded to the south by the hinge zone (iii) The Nile cone, and (iv) The Levant platform.

There is a pronounced flexure zone developed, extending E-W across the mid-Delta area separate between south block and northern subsided basin affecting Pre-Miocene formations and known as the structure Hinge zone (Fig.1A); several East-West trending fault systems that extend into the other regions of Northeast Egypt This structure are dated to the Jurassic crustal break-up of the southern NeoTethys. (Kamel et al. 1998). The Hinge line has shown a predominant effect in all the tectonic and stratigraphic setting of the Nile Delta (Said, 1981).

The NWK gas field lies in the northern central onshore Nile Delta at about 20km from the Egyptian Mediterranean Coast, The discovery of the NWK Field was in 2008 by drilling the NWK 1-1 well. This was followed by three successful wells (NWK1-2, NWK1-3&NWK1-4). The structure depth map on the top of Abu Madi Formation in the NWK Field shows a 3-way dip closure in the hanging wall of a major linked fault of NNW to N-S segments in which NWK1-1, NWK1-3 and NWK 1-2 lie in the eastern part of the field, and NWK1-4 in the western part. This boundary fault extends for more than 12 km from NWK Field in the north to the West Khilala Field at the southeast and delimited at the north with an E-W striking fault of a considerably low displacement (Fig.1 B).

The generalized lithostratigraphic sequence of the Nile Delta ranges in age from Precambrian to Holocene (Fig.2). The Neogene– Quaternary succession is divided into three main sedimentary cycles: Miocene, Plio-Pleistocene, and Holocene (Rizzini et al. 1978; Zaghloul et al.1977a; Kamel et al. 1998). These cycles are dominated by shales and sandstones.

The Miocene-Recent succession in the NWK field includes the top five stratigraphic intervals from the previously recognized stratigraphy of the onshore Nile Delta (Fig. 3). They are arranged in the following order from older to younger, the Messinian sandstones, and the shales intervals of Qawasim and Abu-Madi Formations, and the Pliocene-Pleistocene succession of Kafr El-Sheikh, El-Wastani and Mit-Ghamr formations. The Qawassim Formation is the deepest stratigraphic unit reached by two wells in the NWK field and rests unconformably on Sidi Salem Formation. The Abu Madi formation represent the main reservoir in the study area through two intervals of 50m thick of gas bearing sand, which are unconformably overlain by Pliocene shales with minor sandstones of the Kafr El-Sheikh and El-Wastani formations. The Pleistocene sand and claystone of the Mit- Ghamr Formation rest unconformably on the top of El-Wastani Formation.

3. DATASET AND OBJECTIVE

The NWK gas field has four drilled holes; they are NWK 1-1, NWK1-2, NWK1-3, and NWK1-4, and penetrated the normal stratigraphic succession of the area. The NWK1-1 and NWK1-2 are bottomed in the Qawasim Formation whereas the NWK1-3 and NWK1-4 are bottomed in the Abu-Madi Formation. No major drilling problems were encountered in the shallow intervals except the mud losses due to friable sand, however, in deep intervals within Qawasim formation in NWK1-1 and NWK1-2 an abrupt change in pore pressure and the wells flowed.

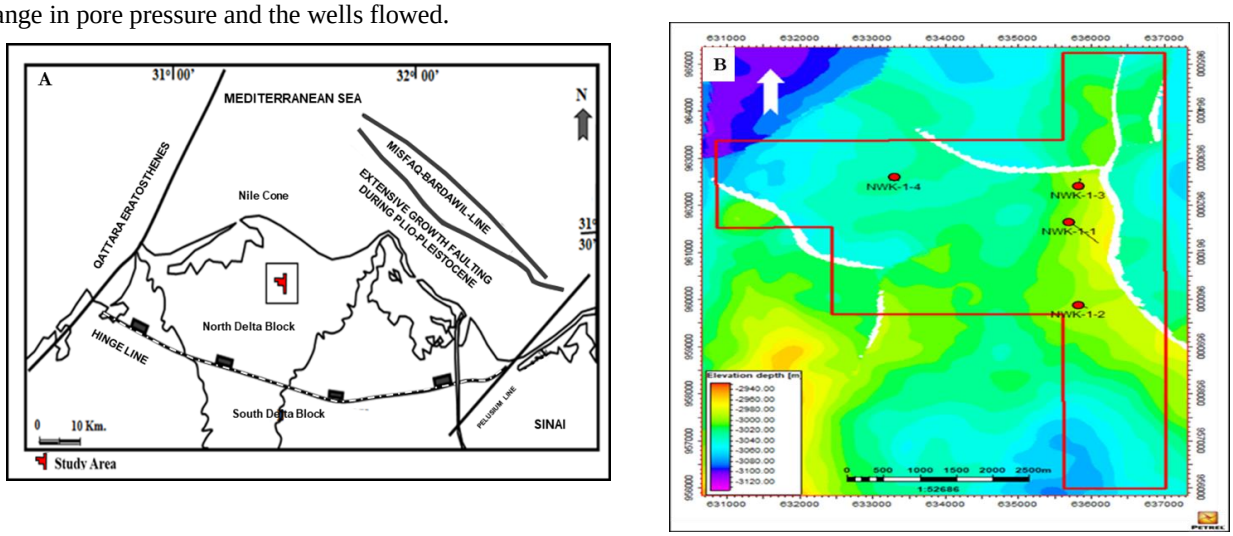

Fig. 1. A)Location map of the study area and regional structure elements of the Nile Delta (after Hemdan et al), and B) depth map on top Abu Madi Fm of the NWK field shoes location of the four boreholes in the area

The studied wells have the traditional well logs data, such as Caliper (CAL), Gamma-ray (GR), Bulk density (RHOB), Compressional slowness (DT), deep, medium, and shallow Resistivity, Neutron porosity (NPHI), and others logs (Table 1). All various log data will be integrated into the present study to construct a 1D PPFG model to be applied to the offset well and the nearby drilling activities in the Nile Delta.

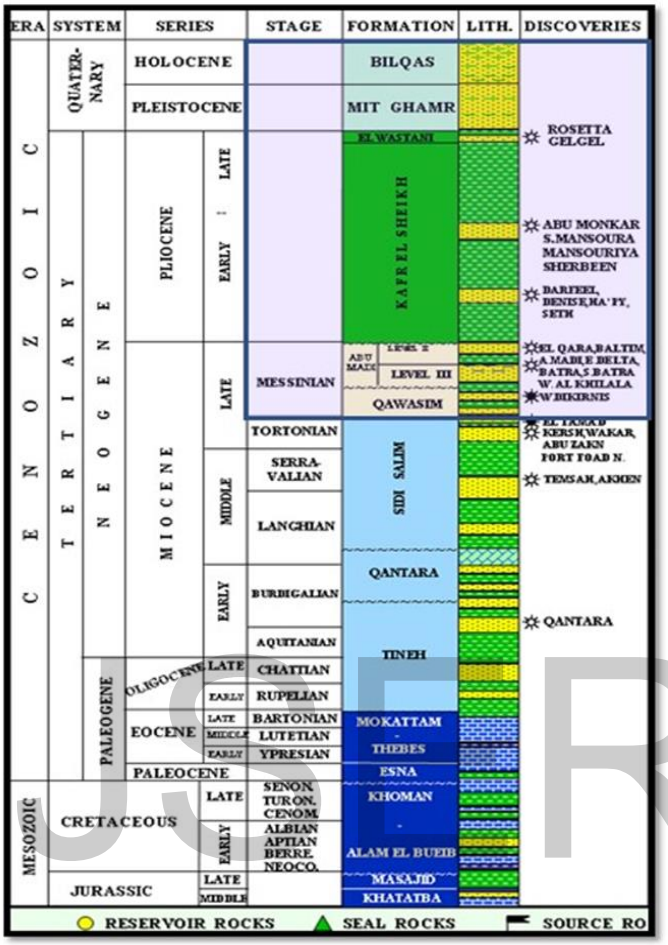

Fig. 2. General stratigraphic column of Nile Delta after EGPC (1994) with the encountered section in NWK Field (burble color highlight).

Table -1: List of the used data in the present work

Data/well	NWK 1-1	NWK 1-2	NWK 1-3	NWK 1-4
Gamma Ray	√	√	√	√
Density & Porosity Logs	√	√	√	√
Resistivity Logs	√	√	√	√
Sonic (DTCO& DTSM)	√	√	√	√
VSP	√		√	
Borehole image	√	√	√	
Direct Pressure Measurements (MDT/XPT/RFT)		√	√	√
Leak of Test (LOT/FIT)		√	√	
Poisson Ratio	√	√	√	√
Drilling reports	√	√	√	√
Composite & Mud logs	√	√	√	√

4. METHODOLOGY AND RESULTS

The present work uses the different empirical methods and the log data of NWK 1-1, NWK 1-3, NWK1-2, and NWK 1-4 wells by the aids of the Techlog platform of Schlumberger to construct the pore pressure and fracture gradients model of the NWK gas field. This objective has been achieved through a workflow of the following four sequential steps:1) The vertical stress or overburden gradient calculation, 2) Shale volume and the normal compaction trend identification, 3) The pore pressure calculation, 4) Fracture gradient calculation, and the resultant models are calibrated with the direct pressure measurements , Mud weight and leak of test.

4.1. VERTICAL STRESS (σv) CALCULATION

Vertical stress (σv) or overburden is the integration of rock density to the depth of interest, and it considers as the core element of the pore pressure model. The magnitude of vertical stress can be derived by the empirical relationships of the bulk density log (RHOB) according to the following equation given by Plumb et al, 1991.

$$\sigma_v = g \int \rho z dz \qquad \textbf{Equation 1}$$

Where: ρ is the density, g is the gravitational acceleration and z is the depth.

Density data has been integrated from well log data where spurious data removed by using DHRO to filter out poor data, interpolation of missing interval then extrapolation to surface.

Techlog extrapolates the density up to the mud line by using the Eq. 2 to have an estimation of the density of the intervals where the log is not available.

$$\rho_{extrapolated} = \rho_{mudline} + A_o\,(TVD - AirGap - WaterDepth)\,\alpha \qquad \textbf{Equation 2}$$

Where $\rho_{mudline}$ is the mud density at the ground level, A_o and α are fitting parameters, and TVD is the true vertical depth. The values used for the calculation are 1.9 g/cm3 of the mud density, 0 m for Water Depth. Figure 6 shows density log of NWK 1-3 well, where densities range from 2.1 to 2.4 g/cc, and plot of depth vs. vertical stress (S_V). The density extrapolated to compensate for data gaps.

The vertical stresses of the studied wells in the NWK field have been calculated and presented as vertical stress to provide a convenient basis for comparison between the wells. All wells display similar vertical stress profiles, the Sv gradient is ~0.97 psi/ft.

4.2. SHALE VOLUME AND NORMAL COMPACTION TREND IDENTIFICATION

The V Shale is based on gamma-ray data used to discriminate between shales and other rock types. In the present study, the V Shale has been calculated by the standard linear interpolation equation:

$$V_{Shale} = V_{Shale} = \frac{GR_{log} - GR_{min}}{GR_{max} - GR_{min}} \qquad \textbf{Equation 3}$$

Where GR log is the log measured gamma-ray value, GR min is the gamma-ray value of clean sand, and GR max is the gamma-ray value of 100% shale deposits (western Atlas international Inc., 1992). GR_{min} and GR_{max} have been determined separately for each formation to obtain the precise value of V_{Shale}.

The normal compaction trend (NCT) reflects properties such, sonic, velocity and resistivity values if the pore pressure were normal (hydrostatic). The normal compaction trend depends on the variation of rock properties with the depth of burial at normal hydrostatic pressure.

Determining the normal compaction trend lines (NCT) for input electrical logs (sonic transit time, velocity and resistivity) or drilling data (d-exponent, sigma log); this line could be determined by empirical methods (Hottman, Eaton, Miller, Bowers, and Zhang) or manually according to the trend of data set in the normal compacted shale formation. The trend of NCT in normal compacted shale interval and any Deviation from the NCT line indicate abnormally pressure shale formation. The NCT line adjusts graphically in shale intervals of sonic and resistivity logs.

The NCT of the four wells in the NWK field was constructed using resistivity and sonic logs for each well, NCT together with Eaton's equation gives a reasonably good pore pressure estimation except in NWK1-2 within Qawasim formation. Then a single normal NCT has been generated to estimate the overpressure magnitude. The application of the single NCT is beneficial to estimate pore pressure for future wells drilled in the study area.

4.3. PORE PRESSURE CALCULATION

Hottmann and Johnson (1965) were probably the first ones to estimate pore pressure from the acoustic travel time/velocity and resistivity well log data of shale. They mentioned that porosity or transit time in shale has an abnormal compaction trend if the fluid pressure is abnormally high according to their data Gardner et al. (1974) proposed equation 2 to predict pore pressure in the following form:

$$p_f = \sigma_v - \frac{(\alpha_v - \beta)(A_1 - B_1 \ln \Delta t)^3}{Z^2} \qquad \textbf{Equation 4}$$

Where Pf is the formation fluid pressure (psi); σv is the overburden stress expressed in psi; αv is the normal overburden stress gradient (psi/ft.); β is the normal fluid pressure gradient (psi/ft); Z is the depth (ft.); Δt is the sonic transit time (μs /ft.); A and B are the constants, A1=82.776 and B1=15.695.
Later, several empirical relationships were presented to predict pore pressure from resistivity, sonic transit time (interval velocity), and other well logging data of shale, among them.

4.3.1. Eaton Methods

Eaton (1972, 1975) based on his work in the Gulf of Mexico, presented the following equation to predict pore pressure P_P in shales using resistivity (Equation 5), interval velocity, and transit time (Equation 6):

$$P_p = \sigma_v - (\sigma_v - P_n)\left(\frac{R}{R_n}\right)^n \qquad \textbf{Equation 5}$$

Where: σv is the vertical stress, R is a value from the resistivity log, Rn is a measurement value assuming that formation is frequently pressured, Pn is the normal pore pressure, n=1.2

$$P_p = \sigma_v - (\sigma_v - P_n)\left(\frac{\Delta t_n}{\Delta t}\right)^n \qquad \textbf{Equation 6}$$

Where: Δt_n is the sonic transit time or slowness in shales, Δt is the sonic transit time in shales obtained from well, n =3

The resistivity (Rn) or transit time (Δt_n) in the NCT needs to be obtained to apply Eaton's method.

4.3.2. Bowers method

Bowers (1995) proposed that the sonic velocity of shale and effective stress have the following power relationship

$$V_p = V_{ml} + A\,\sigma_e^B \qquad \textbf{Equation.7}$$

Where: Vp is the compressional velocity at a given depth; Vml is the compressional velocity in the mudline (i.e., the seafloor or the ground surface, normally Vml ≈5000 ft/s, or 1520 m/s); σe is the vertical effective stress; A and B are the parameters obtained from calibrating regional offset velocity versus effective stress data.

Replacing $\sigma_e = \sigma_v$ - P where the pore pressure P can be obtained from the velocity as described in Eq. (7), as:

$$P = \sigma_v - \left(\frac{V_p - V_{ml}}{A}\right)^{\frac{1}{B}} \qquad \textbf{Equation.8}$$

For Gulf of Mexico wells, A=10–20 and B=0.7–0.75 where P, σv in psi and VP, Vml in ft/s).

Eq. (8) can also be written in terms of transit time simply by substituting 106/ Δt for V_P and 106/ Δtml for Vml:

$$P = \sigma_v - \left(\frac{10^6\left(\frac{1}{\Delta t} - \frac{1}{\Delta t_{ml}}\right)}{A}\right)^{\frac{1}{B}} \qquad \textbf{Equation.9}$$

Where Δtml is the compressional transit time in the mudline, normally Δtml =200 μs/ft or 660 μs/m.

The effective stress and compressional velocity do not follow the loading curve if formation uplift or unloading occurs, and a higher than the velocity in the loading curve appears at the same effective stress. Bowers (1995) proposed the following empirical relation to accounting for the effect of unloading

$$V_p = V_{ml} + A\left[\sigma_{max}\left(\frac{\sigma_e}{\sigma_{max}}\right)^{\frac{1}{U}}\right]^B \qquad \textbf{Equation.10}$$

Where σe, VP, Vml, A and B as before; U is the uplift parameter; and $\sigma_{max} = \left(\frac{V_{max} - V_{ml}}{A}\right)^{\frac{1}{B}}$ ***Equation.11***

Where σmax and Vmax are the estimates of the effective stress and velocity at the onset unloading.
In absence of major lithology changes, Vmax is usually set equal to the velocity at the start of the velocity Reversal. Rearranging Eq. (10) the pore pressure can be obtained for the unloading case:

$$P_{ulo} = \sigma_v - \left(\frac{V_p - V_{ml}}{A}\right)^{\frac{U}{B}} (\sigma_{max})^{1-U} \qquad \textbf{Equation.12}$$

Where Pulo is the pore pressure in the unloading case.

4.3.3. Miller method

The Miller sonic method describes a relationship between velocity and effective stress that can be used to relate sonic/seismic transit time to formation pore pressure. In Miller's sonic method an input parameter "maximum velocity depth", dmax, controls whether unloading has occurred or not. If dmax is less than the depth (Z), unloading has not occurred, the pore pressure can be obtained from the following equation (Zhang et al., 2008):

$$p = \sigma_v - \frac{1}{\lambda}\ln\left(\frac{V_m - V_{ml}}{V_m - V_p}\right)$$ **Equation.13**

Where Vm is the sonic interval velocity in the matrix of the shale (asymptotic travel time at infinite effective stress, Vm=14,000–16,000 ft/s); Vp is the compressional velocity at a given depth; λ is the empirical parameter defining the rate of increase in velocity with effective stress (normally 0.00025); dmax is the depth at which the unloading has occurred.

If dmax≥Z, then unloading behavior is assumed, the pore pressure in the unloading case is calculated from the following equation:

$$p_{ulo} = \sigma_v - \frac{1}{\lambda}\ln\left[a_m\left(1 - \frac{V_p - V_{ulo}}{V_m - V_{ml}}\right)\right]$$ **Equation.14**

Where am is the ratio of slopes of the virgin (loading) and unloading velocities in the effective stress curves σul (normally am=1.8) andnam=vp/vulo; σul is the effective stress from unloading of the sediment; vulo is the velocity where unloading begins.

4.3.4. Tau model

A velocity-dependent pore pressure prediction method was proposed by Shell, which introduced a "Tau" variable into the effective stress equation (Lopez et al., 2004; Gutierrez et al., 2006):

$$\sigma_e = A_s \tau^{B_s}$$ **Equation.15**

where As and Bs are the fitting constants; τ is the Tau variable, and τ= (C−Δt)/ (Δt−D); Δt is the compressional transit time either from the sonic log or seismic velocity; C is the constant related to the mudline transit time (normally C=200 μs/ft), and D is the constant related to the matrix transit time (normally D=50 μs/ft). Then, the pore pressure can be calculated from Eq. (14) using

$$p = \sigma_v - A_s\left(\frac{C - \Delta t}{\Delta t - D}\right)^{B_s}$$ **Equation.16**

According to Gutierrez et al., (2006), the best fitting parameters in the Gulf of Mexico are As =1989.6 and Bs=0.904.
The Tau model and Miller's method are like Bowers' method, but the former has the advantage that both the effects of the matrix and mudline velocities are considered in pore pressure prediction.

4.4. FRACTURE GRADIENT CALCULATION

Fracture pressure is the pressure required to fracture the formation. Fracture gradient can be obtained by dividing the true vertical depth from the fracture pressure.
Fracture gradient is the maximum mud weight; therefore, it is an important parameter for mud weight design in both the drilling planning stage and while drilling. If the mud weight is higher than the formation fracture gradient, then the wellbore will have a tensile failure (be fractured), causing losses of drilling mud or even lost circulation.
Fracture gradient can be measured directly from the downhole leak-off test (LOT) or by the following formula:

$$FG = K(\sigma_v - P_p) + P_p$$ **Equation.17**

Where: FG= Fracture pressure gradient, psi/ft.; σv = the vertical stress, psi; Pp = the pore pressure, psi; K = the stress ratio (unitless), which is the horizontal effective matrix stress over the effective vertical stress.
The fracture gradient methods have only differed in the method of K computation.

4.4.1. Hubbert and Willis' method

The concept and calculation of fracture gradient probably first came from the minimum injection pressure proposed by Hubbert and Willis (1957). They assumed that the minimum injection pressure to hold open and extend a fracture is equal to the minimum stress:

$$P_{inj}^{min} = \sigma_h' + p = \sigma_h$$ **Equation.18**

Where P_{inj}^{min} is the minimum injection pressure; $\tilde{\sigma_h}$ is the effective minimum stress; σ_h is the minimum stress, and p is the pore pressure.

Hubbert and Willis (1957) assumed that under conditions of incipient normal faulting, the effective minimum stress is horizontal and has a value of approximately one-third of the effective overburden stress, i.e $\sigma_h' = \frac{(\sigma_v - P)}{3}$ Therefore, they obtained the minimum injection pressure or fracture pressure in the following form:

$$P_{inj}^{min} = \frac{1}{3}(\sigma_V - P) + P \qquad \textbf{Equation.19}$$

Where σ v is the vertical stress. Later, many empirical and theoretical equations and applications for fracture gradient prediction were presented (Haimson and Fairhurst 1967; Matthews and Kelly 1967; Eaton 1969; Anderson et al. 1973; Althaus 1997; Pilkington 1978; Daines 1982; Breckels and van Eekelen 1982; Constant and Bourgoyne 1988; Aadnoy and Larson 1989; Wojtanowicz et al. 2000; Barker and Meeks 2003; Fredrich et al. 2007; Wessling et al. 2009; Keaney et al. 2010; Zhang 2011; Oriji and Ogbonna 2012). We only review some commonly used methods in the following sections. It should be noted that the Biot coefficient is usually assumed to be 1 in fracture gradient calculation in the oil and gas industry; therefore, the Biot coefficient is not considered in the related equations. In this paper, we follow the same practice except the Biot coefficient has existed in a specific equation.

4.4.2. Matthews and Kelly's method

Matthews Kelly (1967) introduced a variable of the ''matrix stress coefficient (k1),'' equivalent to effective stress coefficient, the method assumes the matrix stress coefficient K to be a function of the vertical effective stress.

4.4.3. K0 (Constant K) method

The user specifies the stress ratio K that best fits the regional stress data directly. The user can use constant values by zone or use a continuous curve by using a "switch variable".

4.4.4. Eaton's method

Eaton (1969) used Poisson's ratio of the formation to calculate the fracture gradient based on the concept of the minimum injection pressure proposed by Hubbert and Willis (1957):

$$K = \nu/(1-\nu) \qquad \textbf{Equation.20}$$

where: ν = is Poisson's ratio

4.4.5. Daines' method

Daines (1982) proposed adding a second term to Eaton's effective stress ratio relation:

$$K = \beta + \frac{\nu}{1-\nu} \qquad \textbf{Equation.21}$$

In most cases, Daines' β term is a correction factor that must be introduced because he used real elastic Poisson's ratios to compute K instead of fictitious ones. Therefore, Daines' equation can be rewritten in the following form:

$$\sigma_f = \left(\beta + \frac{\nu}{1-\nu}\right)(\sigma_V - p) + p \qquad \textbf{Equation.22}$$

4.5. PORE PRESSURE AND FRACTURE GRADIENT MODELLING

Pore pressure value will be estimated using Eaton equations and depending on the normal compaction trend line and the overburden pressure gradient results obtained for each well, the normal pore pressure gradient calculated using sonic and resistivity logs using equations (5&6) calibrated with MDT and used Mud Weight. Then fracture gradient calculated from pore pressure and vertical stress data by Applying K0 with a constant value of 0.61 and Eaton method (Eq. 20) and calibrated with LOT data (Fig. 3&4).

Figures (3&4) display the 1D PPFG model plots of NWK wells in ppg and psi. The analysis shows a cycle of pore pressure regression and transgression. The deviation of pore pressure from the normal limit starts from about ~1900 m TVDss within the Late Pliocene Kafr El-Sheikh formation, (2 overpressured zones are encountered), and increases gradually, the maximum overpressure occurs at the base (~5260 psi). Then followed by a regression cycle in Late Miocene Abu Madi sand (~ 4700 psi), pressure begins to increase again at the basal part of Abu-Madi formation. Thereafter, the pore pressure gradient increases significantly, where a pressure ramp is encountered within Qawasim formation. Fracture gradient estimation by applying K0 with a value of 0.6 and the Eaton Method seems to work reasonably well with LOT data.

Based on the observed pore pressure magnitude, predicted top of the overpressure and geological formation, three pore pressure regimes were identified: 1) A normal-pressure regime in El Wastani interval, 2) overpressured regime with a hydrostatic gradient begins at ~1900mTVDss within Kafr El- Sheikh and continue to Abu-Madi intervals, and 3) an overpressured regime with overpressure gradient in Qawasim interval (change in mud weight 11-16 ppg).

5. DISCUSSION

5.1. PORE PRESSURE VARIATION IN NWK FIELD

Direct measurements (measured pressure and Mud Data) are the most reliable source of information about the fluid pressure inside porous rocks. In NWK field, four wells were analyzed all available data has been put together to study pressure magnitude variation and examine any regional trend. Reservoir pressures in the drilled wells were established by MDT and RFT measurements (Fig.5). These formation pressures were taken from sandstone of Miocene and Pliocene stratigraphy. Formation pressures in the Pliocene Kafr El-Sheikh formation are mostly hydrostatic 2700-4400psi (8.9–9.24 ppg). The late Miocene Abu-Madi upper sand interval are generally regard as moderate overpressure about 4700 psi (9-9.5ppg) except for the severe depletion about 1200 psi (EMW 5-6ppg) encountered at the lower Sand, which indicate compartmentalization nature as the upper zone of virgin pressure and lower zone of depleted pressure. No pressure measurements had taken in late Miocene Qawasim. The mud pressure increases accordingly in Kafr El-Sheikh and Abu-Madi, but in Qawasim exhibits significant increase (11-16 ppg) in NWK 1X and NWK1-2.

In the compaction disequilibrium process, abnormal pore pressure builds up and mud weight is increased accordingly when overpressure is encountered. However, the pore pressure increases for unloading systems usually occurs abruptly. At the onset of unloading, the mud weight must be significantly increased. Accordingly, Kafr El-Sheikh and Abu-Madi overpressurized zones are due to compaction disequilibrium, however, Qawasim overpressurized zone could be due to unloading (vertical transfer and fluid expansion).

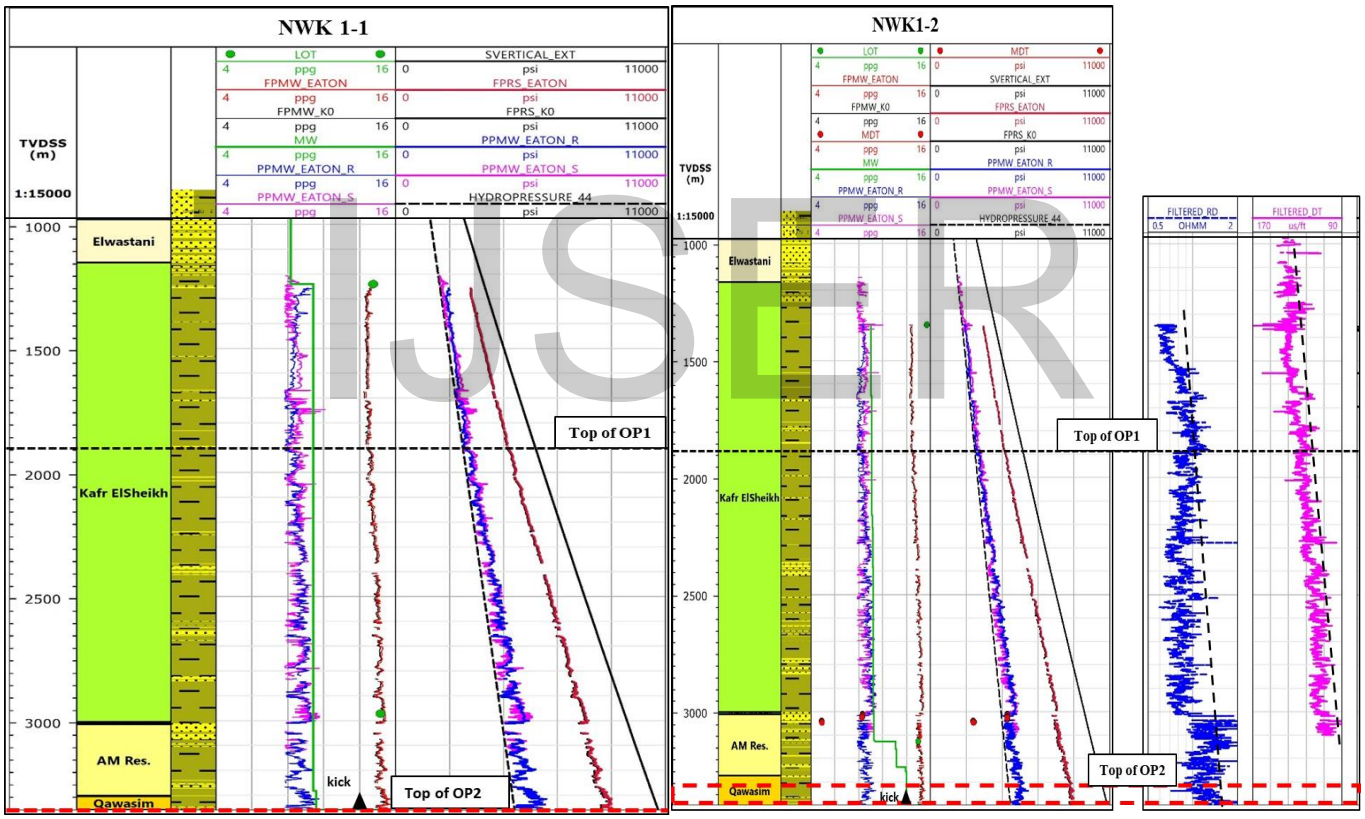

Fig. 3. Overburden, hydrostatic pressure, and the PPFG Plots of the NWK1-1 and NWK-1-2 wells of NWK field. Note the kick in Qawasim Fm in both wells.

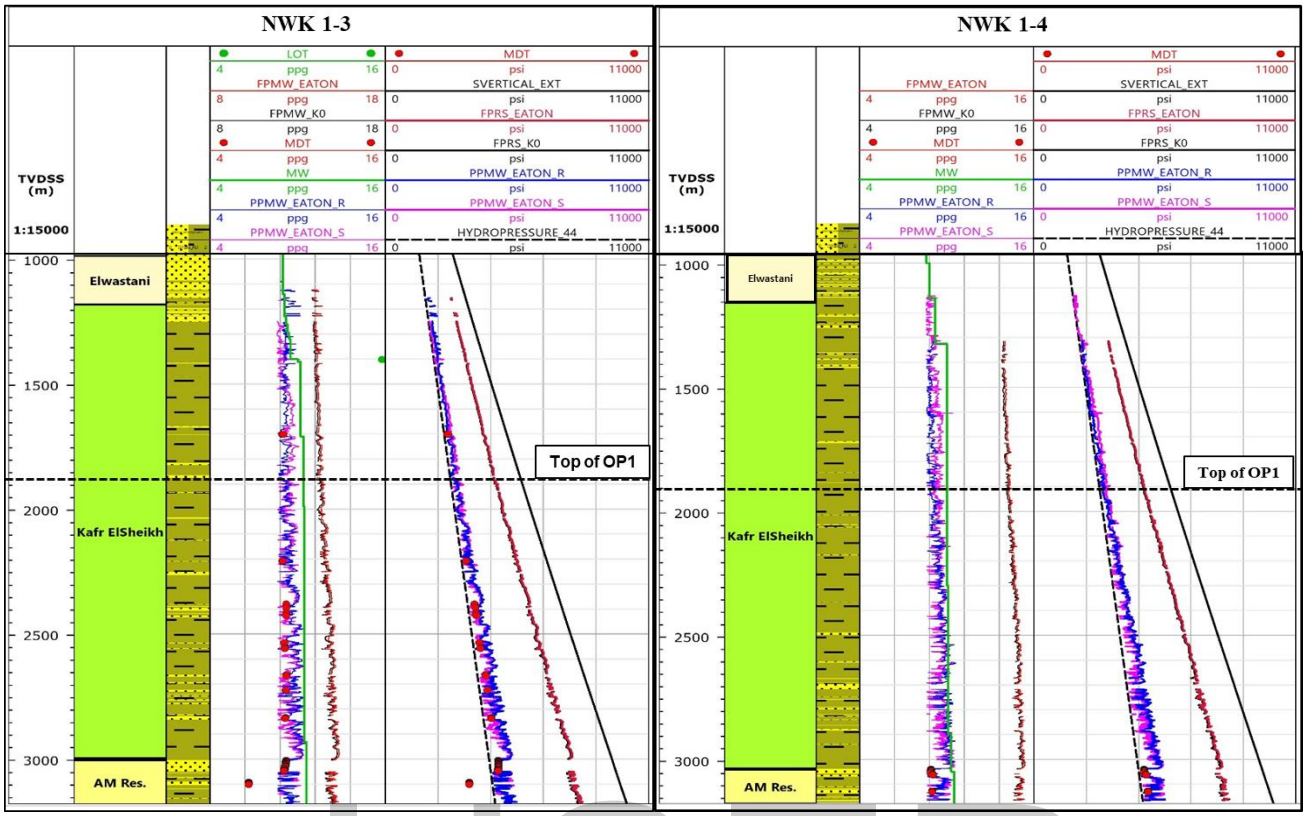

Fig. 4. Overburden, hydrostatic pressure, and the PPFG Plots of the NWK1-1 and NWK-1-2 wells of NWK field. Note the kick in Qawasim Fm in both wells.

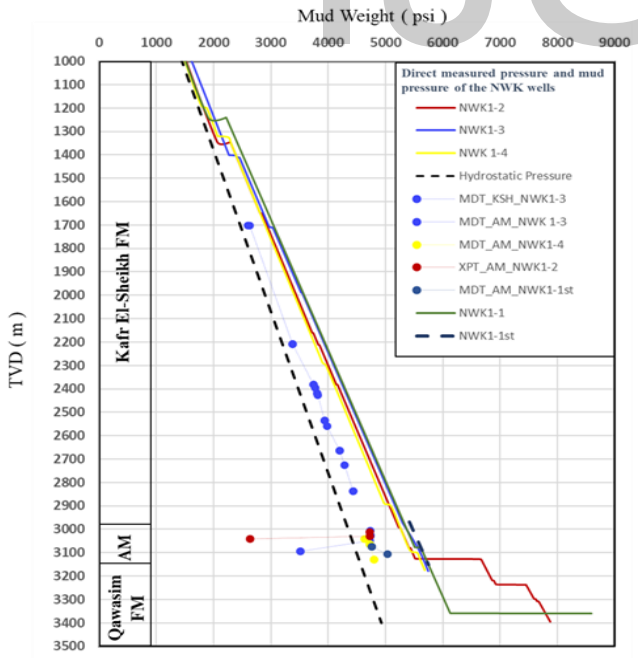

Fig. 5. The directly measured pressure and mud pressures of the NWK wells. Clear abnormalities in mud weight of Qawasim formation

5.2. OVERPRESSURE AND CLAY MINERAL IDENTIFICATION

The clay mineralogy was identified by using Thorium-Potassium Analysis and X-Ray Diffraction (XRD) technique for Kafr El-sheikh and Abu-Madi intervals samples from NWK-1-1 and NWK 1-3 wells. This will help to identify whether a clay diagenesis overpressure mechanism is a plausible cause in NWK field.

By using spectral gamma-ray (SGR) log data, the thorium-potassium cross plots of Schlumberger, 1995 were derived. These cross plots showed that most clays fall in the 'mixed clay' zone, although some data fall within the kaolinite zone, minor chlorite, and very rare amount of illite. The data also indicates no significant pure illite content, which would be expected if clay diagenesis were a major contributor to overpressure (Fig.6).

XRD Clay Fraction analysis carried out (COREX, 2012) to 16 and 19 samples in NWK-1-1 and NWK-1-3 wells. Mineral Composition showed minor to frequent amounts of kaolinite, common amounts of smectite, rare to minor of illite, rare amounts of chlorite are present and illite-smectite mixed-layer are present in some samples (Table.2).

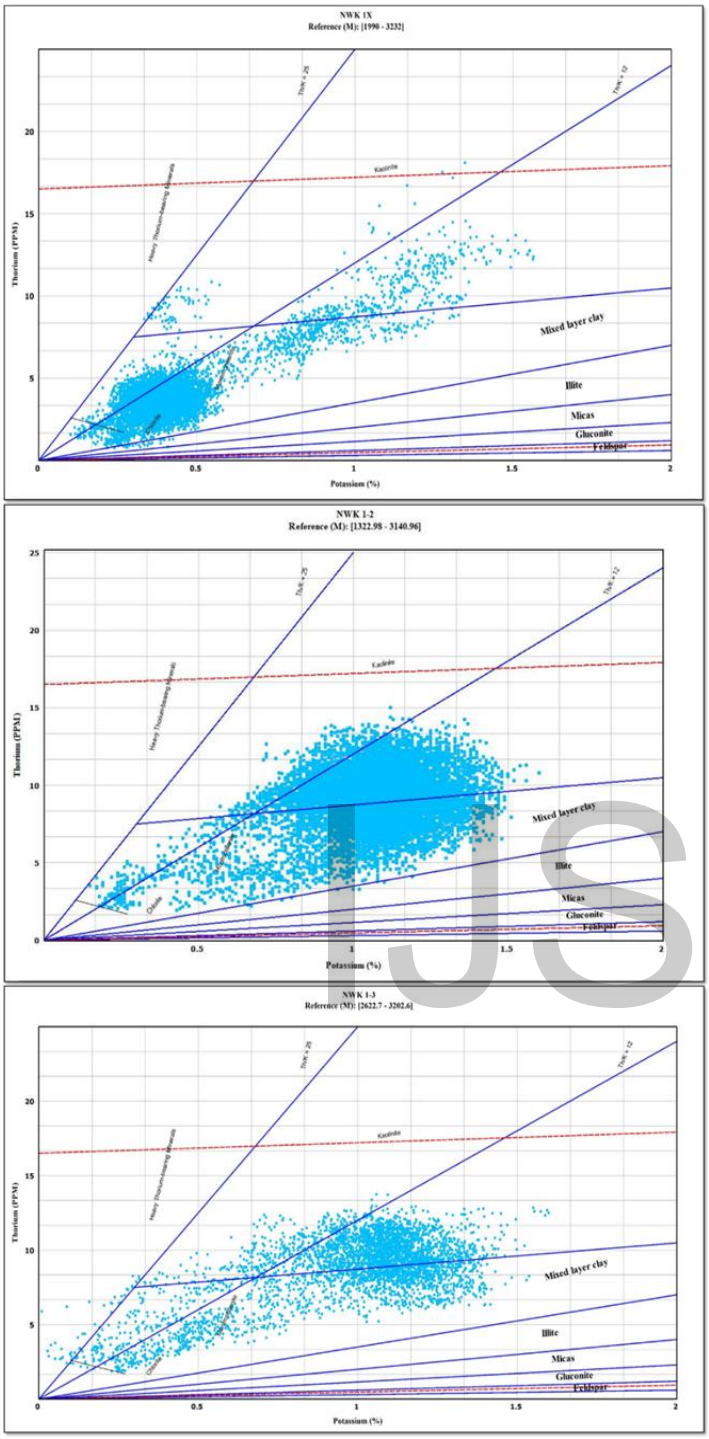

Fig. 6. Thorium –Potassium cross plot based on Schlumberger, LITH-2 chart in 3 wells of Northwest khilala field (NWK 1X, NWK 1-2&NWK 1-3). The majority of the data fall into the mixed clay zone, a part into kaolintic zone and minor amount of Illite to traces in NWK1-X and NWK1-2.

Table -2: Clay Friction

XRD RESULTS (<2 MICRONS CLAY FRACTION)

WELL: NWK-1-1

CORE DEPTH (m)	<2um [wt%]	SMECTITE		ILLITE		CHLORITE		KAOLINITE		ILLITE-SMECTITE	
		A [wt%]	B [wt%]	A [wt%]	B [wt%]	A [wt%]	B [wt%]	A [wt%]	B [wt%]	A [wt%]	B [wt%]
3104.75	37.26	0.00	0.00	6.08	2.27	4.17	1.55	89.75	33.44	0.00	0.00
3105.75	7.82	0.00	0.00	3.45	0.27	5.08	0.40	91.47	7.15	0.00	0.00
3108.00	10.58	0.00	0.00	5.03	0.53	9.31	0.98	85.66	9.07	0.00	0.00
3109.25	10.17	0.00	0.00	2.56	0.26	6.54	0.67	90.90	9.24	0.00	0.00
3114.25	17.75	0.00	0.00	7.85	1.39	5.94	1.05	79.23	14.07	6.98	1.24
3116.00	14.94	0.00	0.00	6.77	1.01	11.28	1.69	81.95	12.24	0.00	0.00
3119.00	8.90	0.00	0.00	3.76	0.33	6.02	0.54	90.22	8.03	0.00	0.00
3125.30	18.44	0.00	0.00	4.65	0.86	6.43	1.19	88.92	16.39	0.00	0.00
3127.00	6.30	0.00	0.00	9.69	0.61	18.54	1.17	71.77	4.52	0.00	0.00
3129.00	30.09	48.15	14.49	20.04	6.03	0.00	0.00	31.81	9.57	0.00	0.00
3129.50	38.89	0.00	0.00	7.46	2.90	5.28	2.05	87.26	33.94	0.00	0.00
3132.00	5.09	0.00	0.00	6.86	0.35	13.72	0.70	79.42	4.04	0.00	0.00
3137.40	2.88	0.00	0.00	7.56	0.22	13.33	0.38	79.11	2.28	0.00	0.00
3139.75	6.70	0.00	0.00	8.70	0.58	8.57	0.57	82.73	5.55	0.00	0.00
3141.50	15.45	0.00	0.00	9.71	1.50	5.78	0.89	84.51	13.06	0.00	0.00
3143.50	12.14	0.00	0.00	7.91	0.96	16.67	2.02	75.42	9.16	0.00	0.00

A% Size Fraction
B% Bulk Sample

XRD RESULTS (<2 MICRONS CLAY FRACTION)

WELL: NWK-1-3

CORE DEPTH (m)	<2um [wt%]	SMECTITE		ILLITE		CHLORITE		KAOLINITE		ILLITE-SMECTITE	
		A [wt%]	B [wt%]	A [wt%]	B [wt%]	A [wt%]	B [wt%]	A [wt%]	B [wt%]	A [wt%]	B [wt%]
3014.50	2.73	_	_	11.32	0.31	_	_	61.32	1.67	27.36	0.75
3017.25	13.95	_	_	15.96	2.27	_	_	84.04	11.68	_	_
3020.00	3.46	_	_	21.92	0.76	_	_	69.41	2.40	8.67	0.30
3025.25	9.66	_	_	10.67	1.03	_	_	89.33	8.63	_	_
3029.00	17.56	_	_	20.30	3.56	_	_	79.70	14.00	_	_
3032.00	3.10	4.79	0.15	21.73	0.67	_	_	61.66	1.91	11.82	0.37
3033.50	6.40	3.22	0.21	13.10	0.84	_	_	74.40	4.76	9.28	0.59
3046.50	8.31	_	_	13.79	1.15	_	_	72.00	5.98	14.21	1.18
3052.00	16.68	2.75	0.95	9.23	1.54	_	_	82.15	13.21	5.87	0.98
3061.70	8.89	0.00	0.00	8.37	0.74	7.31	0.65	84.32	7.50	_	_
3064.00	41.09	51.46	21.14	6.30	2.59	_	_	42.24	17.36	_	_
3065.50	42.68	16.59	7.08	8.90	3.80	_	_	74.51	31.80	_	_
3077.80	66.38	52.17	34.63	7.56	5.02	_	_	40.27	26.73	_	_
3081.80	67.09	27.84	18.68	5.68	3.81	1.60	1.07	64.88	43.53	_	_
3087.68	57.16	39.24	22.43	10.89	6.22	2.29	1.30	47.58	27.20	_	_
3100.50	5.73	_	_	2.96	0.17	_	_	89.78	5.14	7.26	0.42
3106.25	4.35	_	_	2.46	0.11	13.71	0.60	83.83	3.64	_	_
3111.25	2.56	_	_	1.47	0.04	5.23	0.13	93.30	2.39	_	_
3113.25	1.69	_	_	11.17	0.19	20.81	0.35	68.02	1.15	_	_

A%. Size Fraction
B%. Bulk Sample

The performed qualitative analysis performed on NWK field suggests disequilibrium compaction as being the dominant overpressure generation mechanisms (Kafr El-Sheikh and Abu-Madi formations), this conclusion is supported by both the regional geology and rapid sedimentation and burial of sediments during Pliocene time. As well as petrophysical and Th-K cross plot and XRD analyses show Clay diagenesis overpressure mechanism is not plausible.

Our pore pressure estimation models for the four wells in Figures 4 and 5 are in ties with the direct and mud weight measurements (Fig. 5), however, they have the following shortages: 1) non-detection of the severe depletion encountered at the basal part of Abu-Madi sand. 2) the predicated pore pressure in the Qawasim formation interval is lower and not consistent with the actual data (Fig.3).

In NWK1-2 well, Qawasim formation was delineated, as overpressured zone by actual data (Fig.3), however, the typical resistivity log signatures of overpressured sediments were not displayed and do not show reduced values when compared to the normally pressured ones. The explanation of non-detection of overpressure in Qawasim interval by Eaton's method could be referred to 1) the response of resistivity log, which depends upon many factors including mineral composition, type of fluid present in the formation and the fluid retention, or 2) due to contribution of other mechanisms rather than disequilibrium compaction.

The estimated pore pressure in shale sections appear to be overpressured (Fig.3&4) while the intervening sandstones in these intervals are slightly overpressure to hydrostatic as recorded by direct pressure measurement, this confirms the vertical and lateral

pressure compartmentalization, where vertical Separation of upper and lower Abu Madi reservoir and lateral where NWK 1-4 is not in communication with the other wells.

6. COCLUSIONS

According to the present results of pore-pressure and PPFG in the NWK onshore Nile Delta gas field, the following points can be concluded:

In determining the overpressure, a single normal compaction trend (NCT) was generated, which resulted in a reasonably good estimation of overpressure in Kafr El-Sheikh and Abu-Madi intervals. The application of the single NCT is beneficial to estimate pore pressure for future wells drilled in the study area.

Eaton's equation with an exponent coefficient of 1.2, in resistivity, and 0.25, in sonic logs gives the best correlation with mud weight values and MDT/RFT. Overpressure prediction matches the post-drill and easily identified in the Kafr El-Sheikh and Abu-Madi Formations, in contrary of Qawasim formation, where overpressure prediction was not accurate, these sections were drilled with lower mud weight than should be necessary given overpressure conditions, Mud weight ranging 11–16 ppg were used to control the high-pressured zone, these overpressured zones posed drilling problems in NWK 1-1& NWK1-2 wells (lost circulation &well flowed).

In the NWK gas field, three main types of pressure regimes can be identified: 1) A normal-pressure regime, 2) an overpressured regime with a hydrostatic gradient and 3) an overpressured regime with an overpressure gradient.

Fracture gradient Prediction by applying K0 and Eaton Method seems to work reasonably well with LOT data except for Qawasim section.

Disequilibrium compaction is the dominant overpressure generation mechanism in Kafr El-Sheikh and Abu-Madi formations as shown from regional geology and clay contents.

Limitations: 1) non detection of severe depletion encountered at the basal part of Abu Madi Sand. 2) The wireline Resistivity log was not sufficient to identify the pressure ramp within the Qawasim Formation.

7. V. REFERENCE

[1] Althaus VE. (1997). A new model for fracture gradient. J Can Pet Tech. 16(2):99–108.

[2] Barker JW, Meeks WR. (2003). Estimating fracture gradient in Gulf of Mexico deepwater, shallow, massive salt sections. In: SPE annual technical conference and exhibition, 5–8 October, Denver, CO.

[3] Bigelow, E.L. (1992). Introduction to Wireline Log Analysis. Houston, Texas: Western Atlas International.

[4] Bowers, G.L., 1995, Pore Pressure estimation from velocity data; accounting for overpressure mechanisms besides under compaction. SPE Drill Complet, pp.89-95.

[5] Chennakrishnan B. (2008). Pore pressure and Wellbore Stability Analysis of CB-ONN-2002/2 Block in Cambay Basin: presented in GEOINDIA of New Delhi, India, September.

[6] Constant D.W. Bourgoyne A.T. (1988). Fracture-Gradient Prediction for Offshore Wells. SPE Drill Eng.3(136–140).

[7] Corex,2012.PETROGRAPHICAL STUDY FOR WELLS NWK-1-1 & NWK-1-3,NW KHILALA FIELD.

[8] Daines SR. (1982). The prediction of fracture pressures for wildcat wells. JPT. 34(4):863–72.

[9] Eaton, B. A. (1969). Fracture Gradient-Prediction and its Application in Oil field operations: J. Pet. Tech., 10, October 25–32.

[10] Eaton, B.A. (1972). The Effect of Overburden Stress on Geopressures Prediction from Well Logs. Paper SPE3719. JPT, Aug. 1972:929-934.

[11] Eaton B. (1975).The Equation for Geopressure Prediction from Well Logs. Society of Petroleum Engineers, p. 5544. (Eaton Method).

[12] Egyptian General Petroleum Corporation (1994). Nile Delta and North Sinai fields, discoveries, and hydrocarbon potentialities (as a comprehensive overview). EGPC-Cairo, Egypt.

[13] Fertl W. (1976). Abnormal Formation Pressures, Implications to Exploration, Drilling, and Production of Oil and Gas Resources. Elsevier, Amsterdam, 382p.

[14] Gardner, G.F., Gardner, L.W., and Gregory, A.R. (1974). Formation velocity and density – the diagnostic basics for stratigraphic traps: Geophysics, 39, 770-780.

[15] Gutierrez, M. A., Braunsdorf, N. R.. Couzens, B. A (2006). Calibration and ranking of pore-pressure prediction models: The Leading Edge, v. 25, p. 1516–1523.

[16] Hottmann, C.E. and Johnson, R.K. (1965) Estimation of Formation Pressures from Log-Derived Shale Properties. Journal of Petroleum Technology, Vol. 17, No. 06, p.717-722.

[17] Hubbert M.K. Willis D.G. (1957). Mechanics of hydraulic fracturing. PetTrans AIME. 210:153–68.

[18] Kamel, H., Eita, T. and Sarhan, M. (1998). Nile Delta hydrocarbon potentiality. EGPC, 14th Petrol. Exp. Prod. Conf., Cairo, vol. 2, p. 485–503

[19] Law, B. E. Spencer C. W. (1998). Abnormal pressures in hydrocarbon environments, in B. E. Law, G. F. Ulmishek, and V. I. Slavin, eds., AAPG Memoir, 70, 1–11.

[20] Lopez, J.L., Rappold, P.M., Ugueto, G.A., Wieseneck, J.B., Vu, K., (2004). Integrated shared earth model: 3D pore pressure prediction and uncertainty analysis. The Leading Edge, Jan., pp. 52-60.

[21] Matthews, W. R. Kelly, J. (1967). How to Predict Formation Pressure and Fracture Gradient: Oil and Gas Journal, February 20, v. 65, 92 – 1066.

[22] Mouchet, J. C. Mitchell, A. (1989). Abnormal Pressures while Drilling. Editions TECHNIP, Paris, 264p.

[23] Nashaat M. (1998). Abnormally high fluid pressure and seals impacts on hydrocarbon accumulations in the Nile Delta and North Sinai Basins, Egypt, in Law, B.E., G.F. Ulmishek, and V.I.Slavin eds, Abnormal pressure in hydrocarbon environments: AAPG Memoir 70, p. 161-180.

[24] Oriji A, Ogbonna J. (2012). A new fracture gradient prediction technique that shows good results in Gulf of Guinea wells. In: Abu Dhabi international petroleum conference and exhibition, 11–14 November, Abu Dhabi.

[25] Osborne M. Swarbrick R. (1997). Mechanisms for generating overpressure in sedimentary basins: a reevaluation. Am Assoc Pet Geol 81:1023–1041.

[26] Plumb, R. A., K. F. Evans, and T. Engelder (1991), Geophysical log responses and their correlation with bed-to-bed stress contrasts in Paleozoic rocks, Appalachian Plateau, New York, J. Geophys. Res., 96, 14,509–14,528.

[27] Rizzini, A., Vezzani, F., Cococcetta, V. Milad, G. (1978). Stratigraphy and sedimentation of the Neogene-Quaternary section in the Nile Delta area. Mar.Geol, vol.27, pp. 327-348.

[28] Ross D. and Uchupi E. (1977). The structure and sedimentary of the southeastern Mediterranean Sea. – AAPG (Mem.?) 16: 872-709.

[29] Said, R., 1981, The Geology evolution of the River Nile: Springer, New York, N.Y., 151 p.

[30] Said, R., 1990, The Geology of Egypt: Balkema, A.A., Rotterdam, Netherland, 743 p A. A. Reddy and B. N. Chatterji, "A new wavelet based logo-watermarking scheme," Pattern Recognition Letters, vol. 26, pp. 1019-1027, 2005.

[31] Schlumberger, (1995) Log interpretation charts, Schlumberger Ltd., PP. 74-105.

[32] Sestini G. (1989). Nile Delta: depositional environments and geological history. - In: Pickering, K., and Whateley, T. (Eds.): Deltas: sites and traps for fossil fuel. - Geol. Soc. London Spec. Publ. 41: 99-128, Blackwell Scientific Publications, London.

[33] Zaghloul, Z. M. Taha, A. A. and Gheith, A. M., (1977). Microfacies studies and paleoenvironmental trends on the subsurface sediments of Kafr El Sheikh well No. 1, Nile Delta area. - Bull. Mansoura Uni. 5: 113-138

[34] Zhang J, Standifird WB, Lenamond C. (2008). Casing ultradeep, ultralong salt sections in deep water: a case study for failure diagnosis and risk mitigation in record-depth well. In: SPE annual technical conference and exhibition, 21–24 September, Denver, CO,USA;

[35] Zhang J and Yin (2017). Fracture gradient prediction: an overview and an improved method. Petroleum Science.14 (4), 720–730.